ChemComm

Design of a MOF based on octa-nuclear zinc clusters realizing both thermal stability and structural flexibility

Journal:	*ChemComm*
Manuscript ID	CC-COM-10-2021-005893.R2
Article Type:	Communication

Journal Name

COMMUNICATION

Design of a MOF based on octa-nuclear zinc clusters realizing both thermal stability and structural flexibility†

Received 00th January 20xx,
Accepted 00th January 20xx

DOI: 10.1039/x0xx00000x
www.rsc.org/

Yunsheng Ma,*[a,b,‡] Xiaoyan Tang,[a,b,‡] Ming Chen,[a] Akio Mishima,[b] Liangchun Li,[c] Akihiro Hori,[b] Xiaoyu Wu,[d] Lifeng Ding,[d] Shinpei Kusaka [b] and Ryotaro Matsuda*[b]

A octa-nuclear zinc (Zn_8) cluster-based two-fold interpenetrated metal–organic framework (MOF) of $[(CH_3)_2NH_2]_2[Zn_8O_3(FDC)_6]\cdot 7DMF$ (denoted as Zn_8-*as*; H_2FDC = 9H-fluorene-2,7-dicarboxylic acid; DMF = *N*,*N*-dimethylformamide) was synthesized by reactions of a hard base of a curved dicarboxylate ligand (H_2FDC) with the borderline acid of Zn(II) under solvothermal conditions. Zn_8-*as* shows significant crystal volume shrinkage upon heating, yielding solvate-free framework of $[(CH_3)_2NH_2]_2[Zn_8O_3(FDC)_6]$ (Zn_8-*de*). Zn_8-*de* displays gated adsorption for C_2H_2 and type-I adsorption for CO_2, attributed to the framework flexibility and the different interactions between the gas molecules and the host framework.

Flexible metal-organic frameworks (MOFs) are a subclass of MOF materials that are dynamic and capable of reversible transformation upon external stimuli, such as guest removal/exchange, vacuum, photo-irradiation, mechanical forces, and thermal treatment.[1] Since the organic ligands and inorganic metal-based (cluster) nodes are the two basic components of MOFs, it remains effective to modulate the flexibility of MOFs by increasing the softness of ligands, such as the introduction of a long ligand or the installation of a dangling pendant.[2-4] On the contrary, the intermolecular interactions between the organic linkers in a MOF serve to enhance the stability while diminishing the flexibility of the framework.[5] Creating stable MOFs that are flexible have thus attracted broad interest in gas sensing and separation.[6]

The nature of the coordination bonds plays an important role in the stability of MOFs.[7] According to the hard-soft-acid-base theory in coordination chemistry, the borderline acid Zn(II) and the hard base carboxylate only provide relatively weak Zn-O coordination which is susceptible to competitive coordination from solvent (i.e. H_2O).[8] Nevertheless, the formation of polynuclear cluster nodes in MOFs enhances the connectivity, thus ensure architectural and thermal stability. The collective existence of multiple somewhat 'weak' metal-ligand interactions may benefit the displacive phase transition reflecting structural flexibility.

Several Zn-based polynuclear nodes, such as dinuclear paddle-wheel $Zn_2(COO)_4$,[9] trinuclear $[Zn_3(COO)_6]$ (linear)/$[Zn_3(\mu_3\text{-O})(COO)_6]$ (triangular),[10] tetrahedral $[Zn_4(\mu_3\text{-O})(COO)_6]$[11] cores are widely found as the secondary building units (SBUs) in flexible frameworks.[12] However, MOFs with higher-nuclearity Zn-based SBUs, e.g. penta-,[13] hexa-,[14] hepta-,[15] octanuclear,[16] and other high nuclearity clusters[17] remains scarce, and the flexibility in some of these MOFs were showcased exclusively from the gas adsorption isotherms.

Much work has been devoted to the rational design of MOFs with specific structures. Linear dicarboxylate ligand with different rigid spacers (e.g., benzene, naphthalene, biphenyl) have been used to generate isoreticular frameworks (IRMOFs) containing $[Zn_4(\mu_3\text{-O})(COO)_6]$ cores.[11d] Nolinear ligands with 120° or 90° bond angles of the dicarboxylate groups could generate not only MOFs but also metal-organic polyhedra (MOPs).[18] 9H-fluorene-2,7-dicarboxylic acid (H_2FDC, S1-S6) is one kind of nolinear ligand with the bond angle of 156°.[19] Surprisingly, a 3D Kagomé MOF bearing $[Zn_4(\mu_3\text{-O})(COO)_6]$ was obtained in DMSO and ethanol.[19b] Clearly, the bond angles of the ligands and solvent play important roles for the formation of the specific compounds. In this work, we demonstrate the generation of a octanuclear Zn-based MOF of $[(CH_3)_2NH_2]_2[Zn_8O_3(FDC)_6]\cdot 7DMF$ (denoted as **Zn_8-*as***) assembled from H_2FDC and $Zn(NO_3)_2\cdot 6H_2O$ (ESI†) in DMF and H_2O. Here, H_2O plays important role for the formation of

[a] School of Materials Engineering, Jiangsu Key Laboratory of Advanced Functional Materials, Changshu Institute of Technology, Changshu, Jiangsu 215500, China. Email:myschem@hotmail.com
[b] Department of Materials Chemistry, Graduate School of Engineering, Nagoya University, Chikusa-ku, Nagoya 464-8603, Japan. Email: ryotaro.matsuda@chembio.nagoya-u.ac.jp
[c] Shanghai Key Lab of Chemical Assessment and Sustainability, School of Chemical Science and Engineering, Tongji University, Shanghai 200092, China
[d] Department of Chemistry, Xi'an JiaoTong-Liverpool University, 111 Ren'ai Road, Suzhou Dushu Lake Higher Education Town, Jiangsu Province, 215123, China

† Electronic Supplementary Information (ESI) available: Synthetic methods, characterization data, additional tables and figures. CCDC 2106380 and 2106381. For ESI and crystallographic data in CIF or other electronic format see DOI: 10.1039/x0xx00000x

‡These authors contributed equally to this work.

polynuclear node. We also structurally characterized the desolvated form of the framework, *viz.*, $[(CH_3)_2NH_2]_2[Zn_8O_3(FDC)_6]$ (**Zn_8-*de***), providing direct insight on structural flexibility and toward the distinctive adsorption behaviors and thus its separation potential of two industrially important gases of C_2H_2 and CO_2.

The structure of **Zn_8-*as*** features a three-dimensional (3D) jungle-gym-like framework with $[Zn_8O_3]^{10+}$ core as "joints" and FDC^{2-} as the "struts" (Fig. 1). The overall framework is anionic and the $[(CH_3)_2NH_2]^+$ cations originating from the decomposition of DMF serve as the counterions for charge balance.[20] The presence of $[(CH_3)_2NH_2]^+$ was further confirmed by thermogravimetric analysis (TGA) (Fig. S7 and S8), ^1H and ^{13}C nuclear magnetic resonance (NMR) measurements (Figs. S9 – S12). TGA shows a one-step weight loss (19.5%) in the temperature range of 25−190 °C, corresponding to the removal of seven DMF solvates (calculated 19.6%). Meanwhile, the subsequent weight loss (3.5%) from 190−370 °C, corresponds to the removal of two $[(CH_3)_2NH_2]^+$ cations (calculated 3.5%). Rapid weight loss occurs when the temperature over 400 °C, which is close to that of MOF-5.[21] The DMSO-d_6 and DCl digested sample of **Zn_8-*as*** shows a peak at 2.46 ppm (CH_3), resembling that found in the commercially available $[Me_2NH_2]Cl$ in DMSO-d_6 (2.48 ppm). Besides, a peak at 34.42 ppm in the ^{13}C NMR of $[Me_2NH_2]Cl$ further confirms the correct assignment of the peak at 34.63 ppm as the methyl group.

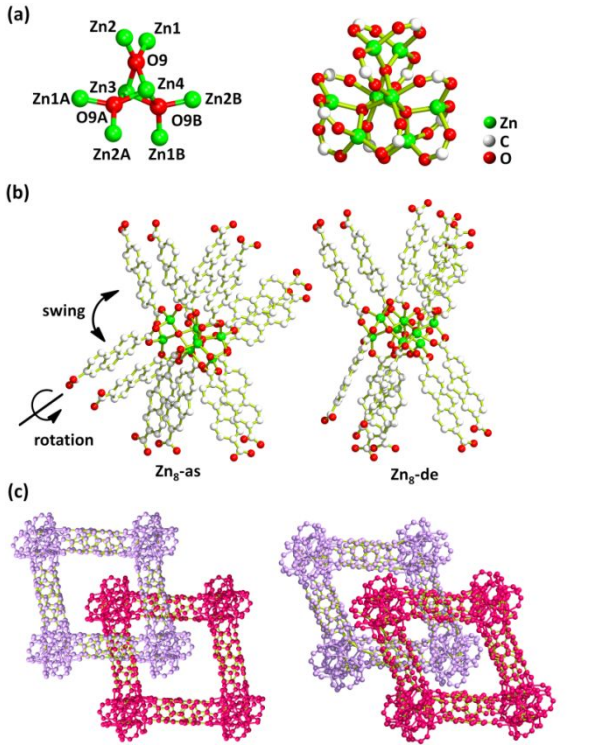

Fig. 1 Crystal structures of **Zn_8-as** and **Zn_8-de**. (a) The $[Zn_8O_3]^{10+}$ and $[Zn_8O_3(O_2C)_6]^{2-}$ core structures. (b) The SBUs of **Zn_8-as** and **Zn_8-de** showing the full coordination of the Zn^{2+} and the configurational differences between the two SBUs. (c) Box structural motif of **Zn_8-as** and **Zn_8-de** with two-fold interpenetrated structures. All hydrogen atoms are omitted for clarity. Color codes in (b): zinc, green; oxygen, red; carbon, white.

The $[Zn_8O_3]^{10+}$ core has a three-fold symmetry featuring a Zn···Zn axis and can be readily considered as fused by three $[Zn_4O]^{6+}$ subunits via merging a pair of Zn from each unit (Fig. 1a). The $[Zn_8O_3]^{10+}$ core also functions as a twelve-connected node (Fig. 1b) to associate with the FDC^{2-} ligands to give a cationic 3D MOF sharing the same topology as that of MOF-5 but with a two-fold interpenetration.[11c] The PLATON calculation suggests that this material has a free accessible volume of about 37.4% (12192 Å^3 of the 32565 Å^3 per unit cell volume).[22]

Upon activation, the powder X-ray diffraction (PXRD) pattern for the guest-free sample (**Zn_8-*de***) is different from that of **Zn_8-*as***, indicating the structural flexibility (Fig. S13). Fortunately, the quality of the **Zn_8-*de*** single crystals still allows us to perform X-ray diffraction characterization to obtain accurate information of its atomic connectivity which is critical to elucidate the gas uptake mechanisms. Compared with the structure of the **Zn_8-*as***, the unit cell of **Zn_8-*de*** displays remarkable changes ($-\Delta a/a$ = 16.5%, $\Delta c/c$ = 12.4%, $-\Delta V/V$ = 21.3%) (Table S1). The structure of **Zn_8-*de*** also shows significant framework distortion as compared to **Zn_8-*as*** (Fig. 1c). The obvious changes in the coordination geometry at Zn^{2+} centers were observed, which is associated with a substantial reorientation of FDC^{2-} ligands. The dihedral angle between the FDC^{2-} planes changed from 77.526° to 120.004°, indicating swing of these FDC^{2-} ligands to the Zn···Zn axis together with the rotation of the fluorene planes of the linkers.

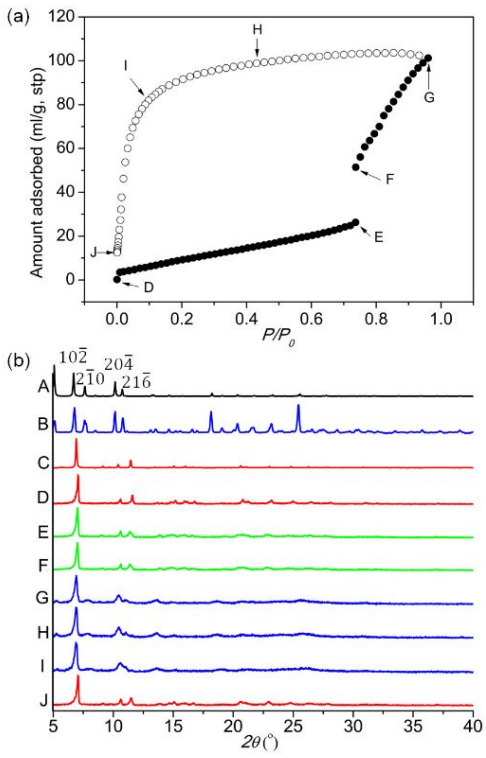

Fig. 2 (a) C_2H_2 adsorption (●) and desorption (○) profiles of **Zn_8-*de*** at 189.5 K. (b) The PXRD patterns of **Zn_8-*as*** and **Zn_8-*de***. Lanes A and C: the simulated pattern of **Zn_8-*as*** and **Zn_8-*de*** based on X-ray structure diffraction data; lane B: the experimental pattern of **Zn_8-*as*** measured at ambient temperature; lanes D–J: the patterns of **Zn_8-*de*** measured under C_2H_2 sorption. In lanes D–J, each pattern corresponds to the points labeled in (a). Cu-Kα radiation was used for all the PXRD measurements.

There is intense contemporary interest in developing materials for highly efficient CO_2/C_2H_2 separation.[23] The gas adsorption properties of **Zn_8-*de*** were then studied for N_2 at 77.0 K, CO_2 at 194.7 K, and C_2H_2 at 189.5 K using the crystalline powder. For N_2, no appreciable adsorption could be observed due to the slow diffusion of N_2 (Fig. S14). Notably, the C_2H_2 isotherm shows gated adsorption with a large hysteresis, which is in good agreement with the structural flexibility (Fig. 2a). The gate-opening pressure is about 0.75 bar with saturated adsorption amount to around 100 $cm^3\ g^{-1}$ at standard pressure. The gated adsorption process was reflected in the *in situ* coincident PXRD/adsorption measurement (lanes D–G in Fig. 2b). Compared with the patterns of **Zn_8-*as***, the peaks of **Zn_8-*de*** shifted to high angles, indicating that the framework contracted upon activation. The peaks in the PXRD patterns become broad between lanes D and E, which indicates that the structural transformation occurred in a non-uniform fashion in response to the adsorption of C_2H_2. From point F to point G, an exponential uptake of C_2H_2 can be observed, accompanied by a significant change in the PXRD at $10\overline{2}$, $2\overline{1}0$, $20\overline{4}$ and $2\overline{1}6$. The shifting peaks at $10\overline{2}$ and $2\overline{1}6$ are related to the deformation of the framework. The appearance of new broad peaks in PXRD pattern at point G, indicating that the C_2H_2-loaded framework is going to reach the saturated form of a framework like **Zn_8-*as*** (Fig. S15).

The gated-adsorption of **Zn_8-*de*** for C_2H_2 should be related to its flexible anionic framework. As **Zn_8-*de*** has isolated cavities, and the diffusion of rod-shaped C_2H_2 into the pore is expected to be slow. The gas molecules cannot move freely into the small pore but are forced to keep their orientation during diffusion until a sudden structural expansion occurs.

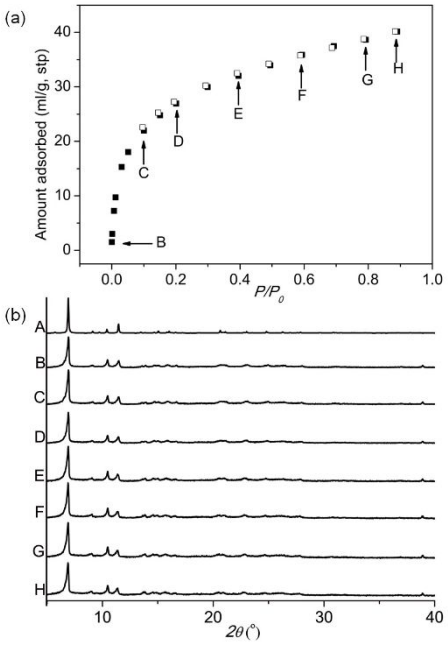

Fig. 3 (a) CO_2 adsorption (■) and desorption (□) profiles of **Zn_8-de** at 194.7 K. (b) A: the simulated pattern of the single-crystal structure of **Zn_8-de**, B–H: PXRD patterns of **Zn_8-de** measured under CO_2 sorption. Each pattern corresponds to the points labeled in the isotherm. Cu-Kα radiation was used for all of the measurements.

Since CO_2 and C_2H_2 have the same kinetic diameter but opposite quadruple moment around the rod-shaped entity,[14] the study of CO_2 adsorption of **Zn_8-*de*** could give more insight on the structural features of **Zn_8-*de*** as well as the nature of their pores. The measurement result shows that **Zn_8-*de*** exhibits a reversible type-I adsorption isotherm for CO_2 with the saturated adsorption amount of 40 $cm^3\ g^{-1}$ (Fig. 3a). No obvious structural expansion was observed with the adsorption of CO_2 as confirmed from the *in situ* PXRD and adsorption (Fig. 3b). The different isotherms on C_2H_2 and CO_2 indicates that C_2H_2 has a stronger interaction with the nanopore, while CO_2 can easily penetrate the nanopore.

Moreover, density functional theory (DFT) calculation confirms that both C_2H_2 and CO_2 are located in the center of microporous cages surrounded by the two interpenetrated frameworks of **Zn_8-*as*** and **Zn_8-*de*** (Fig. S16), where C_2H_2 binding in **Zn_8-*de*** shows a higher binding energy (34.22 kJ mol^{-1}) than that of CO_2 (30.76 kJ mol^{-1}) in **Zn_8-*de***. The C_2H_2 binding affinity in **Zn_8-*as*** is increased to 39.73 kJ mol^{-1} after the expansion to compensate for the energy change induced by structure recovery. The distance between the centroid of the optimized C_2H_2 and Zn site in **Zn_8-as** is closer than that of **Zn_8-de** (4.846 Å < 5.647 Å), while the distance between the C_2H_2 and organic backbone unit is larger in **Zn_8-as** than **Zn_8-de** (4.105 Å > 3.257 Å), this is due to that the adsorption affinity of C_2H_2 and CO_2 is more dominated by strong electrostatic interaction provided by Zn site (ESI†).

In conclusion, we demonstrated that the Zn_8 based MOF showed extremely high thermal stability and high structural flexibility. The flexibility should arise from the hard-soft properties of Zn and O atoms, while the stability should be the presence of multiple Zn-O bonds in the polynuclear node. **Zn_8-*de*** showed the gated adsorption for C_2H_2 and type-I adsorption for CO_2, respectively, which shows that **Zn_8-*de*** can be a potential gas separation material. This finding should be useful for constructing flexible and stable MOFs with promising gas separation properties.

This work is supported by the CREST (Grant No. JPMJCR17I3) of the Japan Science and Technology Agency (JST), and JSPS KAKENHI (Grant No. JP18K14043, JP19H02734, JP20K20564). Y. M. thanks for the financial support by SF of Suzhou (No. SS2019030) China. L. D. thanks for the financial support by the Xi'an Jiaotong-Liverpool University (XJTLU) Research Development Funds (RDF-15-01-23 and RDF-16-02-03), and the Key Program Special Fund in XJTLU (KSF-E-03).

Conflicts of interest

There are no conflicts to declare.

Notes and references

1 (a) T. L. Easun, F. Moreau, Y. Yan, S. Yang and M. Schröder, *Chem. Soc. Rev.*, 2017, **46**, 239—274; (b) X.-G. Wang, L. Xu, M.-J. Li and X.-Z. Zhang, *Angew. Chem. Int. Ed.*, 2020, **59**, 18078—18086; (c) T. Kundu, M. Wahiduzzaman, B. B. Shah, G. Maurin and D. Zhao, *Angew. Chem. Int. Ed.*, 2019, **58**, 8073—8077; (d) K. Roztocki, F. Formalik, A. Krawczuk, I. Senkovska, B. Kuchta, S. Kaskel and D. Matoga, *Angew.*

Chem. Int. Ed., 2020, **59**, 4491—4497; (e) Z.-X. Zhang, N.-N. Ding, W.-H. Zhang, J.-X. Chen, D. J. Young and T. S. A. Hor, *Angew. Chem. Int. Etd.*, 2014, **53**, 4628—4632; (f) S. Horike, S. Shimomura and S. Kitagawa, *Nat. Chem.*, 2009, **1**, 695—704; (g) J.-P. Zhang, H.-L. Zhou, D.-D. Zhou, P.-Q. Liao and X.-M. Chen, *Nat. Sci. Rev.*, 2018, **5**, 907–919.

2 S. Y. Liu, D. D. Zhou, C. T. He, P. Q. Liao, X. N. Cheng, Y. T. Xu, J. W. Ye, J. P. Zhang and X. M. Chen, *Angew. Chem. Int. Ed.*, 2016, **55**, 16021—16025.

3 Z. Chang, D.-H. Yang, J. Xu, T.-L. Hu and X.-H. Bu, *Adv. Mater.*, 2015, **27**, 5432—5441.

4 Z.-J. Lin, J. Lu, M. Hong and R. Cao, *Chem. Soc. Rev.*, 2014, **43**, 5867—5895.

5 (a) G. Chang, B. Li, H. Wang, T. Hu, Z. Bao and B. Chen, *Chem. Commun.*, 2016, **52**, 3494—3496; (b) D.-D. Zhou, Z.-J. Liu, C.-T. He, P.-Q. Liao, H.-L. Zhou, Z.-S. Zhong, R.-B. Lin, W.-X. Zhang, J.-P. Zhang and X.-M. Chen, *Chem. Commun.*, 2015, **51**, 12665—12668; (c) L. Qin, Z.-M. Ju, Z.-J. Wang, F.-D. Meng, H.-G. Zheng and J.-X. Chen, *Cryst. Growth Des.*, 2014, **14**, 2742—2746.

6 (a) M.-Y. Chao, J. Chen, X.-Y. Wu, R.-Y. Wang, P.-P. Wang, L. Ding, D. J. Young and W.-H. Zhang, *ChemPlusChem*, 2020, **85**, 503—509; (b) Y. Zhang, X. Zhang, J. Lyu, K.-i. Otake, X. Wang, L. R. Redfern, C. D. Malliakas, Z. Li, T. Islamoglu, B. Wang and O. K. Farha, *J. Am. Chem. Soc.*, 2018, **140**, 11179—11183.

7 (a) Y.-X. Shi, W.-X. Li, W.-H. Zhang and J.-P. Lang, *Inorg. Chem.*, 2018, **57**, 8627–8633; (b) I. Abánades Lázaro, C. J. R. Wells and R. S. Forgan, *Angew. Chem. Int. Ed.*, 2020, **59**, 5211—5217; (c) F. Hillman, M. R. A. Hamid, P. Krokidas, S. Moncho, E. N. Brothers, I. G. Economou and H.-K. Jeong, *Angew. Chem. Int. Ed.*, 2021, **60**, 10103—10111; (d) M. Hayashi, D. T. Lee, M. D. de Mello, J. A. Boscoboinik and M. Tsapatsis, *Angew. Chem. Int. Ed.*, 2021, **60**, 9316—9320; (e) H. Yin, J. Shang, J. Choi and A. C. K. Yip, *Micropor. Mesopor. Mater.*, 2019, **280**, 347—356.

8 (a) C. K. Brozek, V. K. Michaelis, T.-C. Ong, L. Bellarosa, N. López, R. G. Griffin and M. Dincă, *ACS Cent. Sci.*, 2015, **1**, 252–260; (b) S. S. Kaye, A. Dailly, O. M. Yaghi and J. R. Long, *J. Am. Chem. Soc.*, 2007, **129**, 14176—14177; (c) Y. Liu, S.-X. Lin, R.-J. Niu, Q. Liu, W.-H. Zhang and D. J. Young, *ChemPlusChem*, 2020, **85**, 832—837; (d) J.-X. Chen, M. Chen, N.-N. Ding, W.-H. Chen, W.-H. Zhang, T. S. A. Hor and D. J. Young, *Inorg. Chem.*, 2014, **53**, 7446—7454.

9 (a) O. M. Yaghi, C. E. Davis, G. Li and H. Li, *J. Am. Chem. Soc.*, 1997, **119**, 2861—2868; (b) H. Li, M. Eddaoudi, T. L. Groy and O. M. Yaghi, *J. Am. Chem. Soc.*, 1998, **120**, 8571—8572; (c) Z. Hu, K. Tan, W. P. Lustig, H. Wang, Y. Zhao, C. Zheng, D. Banerjee, T. J. Emge, Y. J. Chabal and J. Li, *Chem. Sci.*, 2014, **5**, 4873—4877.

10 (a) C. A. Bauer, T. V. Timofeeva, T. B. Settersten, B. D. Patterson, V. H. Liu, B. A. Simmons and M. D. Allendorf, *J. Am. Chem. Soc.*, 2007, **129**, 7136—7144; (b) J. Sun, Y. Zhou, Q. Fang, Z. Chen, L. Weng, G. Zhu, S. Qiu and D. Zhao, *Inorg. Chem.*, 2006, **45**, 8677–8684; (c) A. K. Chaudhari, H. J. Kim, I. Han and J.-C. Tan, *Adv. Mater.*, 2017, **29**, 1701463; (d) K. Sokolowski, W. Bury, I. Justyniak, D. Fairen-Jimenez, K. Soltys, D. Prochowicz, S. Yang, M. Schroeder and J. Lewinski, *Angew. Chem. Int. Ed.*, 2013, **52**, 13414—13418.

11 (a) M. M. Li and M. Dincă, *ACS Appl. Mater. Interfaces*, 2017, **9**, 33528—33532; (b) S. Y. Zhang, D. Li, D. Guo, H. Zhang, W. Shi, P. Cheng, L. Wojtas and M. J. Zaworotko, *J. Am. Chem. Soc.*, 2015, **137**, 15406—15409; (c) H. Li, M. Eddaoudi, M. O'Keeffe and O. M. Yaghi, *Nature*, 1999, **402**, 276—279; (d) M. Eddaoudi, J. Kim, Rosi, N.; D. V. J. Wachter, M. O'Keeffe, O. M. Yaghi, *Science*, 2002, **295**, 469–472.

12 (a) N. Chatterjee and C. L. Oliver, *Cryst. Growth Des.*, 2018, **18**, 7570—7578; (b) S. K. Elsaidi, M. H. Mohamed, D. Banerjee and P. K. Thallapally, *Coord. Chem. Rev.*, 2018, **358**, 125—152; (c) A. Schneemann, V. Bon, I. Schwedler, I. Senkovska, S. Kaskel and R. A. Fischer, *Chem. Soc. Rev.*, 2014, **43**, 6062—6096; (d) Y. Sakata, S. Furukawa, M. Kondo, K. Hirai, N. Horike, Y. Takashima, H. Uehara, N. Louvain, M. Meilikhov, T. Tsuruoka, S. Isoda, W. Kosaka, O. Sakata and S. Kitagawa, *Science*, 2013, **339**, 193—196; (e) G. Férey and C. Serre, *Chem. Soc. Rev.*, 2009, **38**, 1380—1399; (f) L. Sarkisov, R. L. Martin, M. Haranczyk and B. Smit, *J. Am. Chem. Soc.*, 2014, **136**, 2228—2231.

13 Q.-R. Fang, G.-S. Zhu, Z. Jin, M. Xue, X. Wei, D.-J. Wang and S.-L. Qiu, *Cryst. Growth Des.*, 2007, **7**, 1035—1037.

14 J. Cui, Y. Li, Z. Guo and H. Zheng, *Chem. Commun.*, 2013, **49**, 555—557.

15 Q.-R. Fang, G.-S. Zhu, M. Xue, Q.-L. Zhang, J.-Y. Sun, X.-D. Guo, S.-L. Qiu, S.-T. Xu, P. Wang, D.-J. Wang and Y. Wei, *Chem. – Eur. J.*, 2006, **12**, 3754—3758.

16 Y.-Q. Lan, S.-L. Li, K.-Z. Shao, X.-L. Wang, D.-Y. Du, Z.-M. Su and D.-J. Wang, *Cryst. Growth Des.*, 2008, **8**, 3490—3492.

17 Y.-W. Li, K.-H. He and X.-H. Bu, *J. Mater. Chem. A*, 2013, **1**, 4186—4189.

18 (a) H. Sato, W. Kosaka, R. Matsuda, A. Hori, Y. Hijikata, R. V. Belosludov, S. Sakaki, M. Takata and S. Kitagawa, *Science*, 2014, **343**, 167–170; (b) J. R. Li and H. C. Zhou, *Nat. Chem.*, 2010, **2**, 893–898.

19 (a) Y. Ma, Y. Harada, A. Hori, Y. Hijikata, L. Li and R. Matsuda, *Dalton Trans.*, 2017, **46**, 15200—15203; (b) Q. Yue, Q. Sun, A. L. Cheng and E. Q. Gao, *Cryst. Growth Des.*, 2010,**10**, 44–47.

20 S. Hausdorf, F. Baitalow, J. Seidel and F. O. R. L. Mertens, *J. Phys. Chem. A*, 2007, **111**, 4259—4266.

21 J. Sun, Q. Wei, P. Song, Z. Yang and Q. Wang, *J. Mater. Sci.: Mater in Electr.,* 2019, **31**, 837–847.

22 A. L. Spek, *Acta Crystallogr., Sect. C*, 2015, **71**, 9—18.

23 (a) Z. Niu, X. Cui, T. Pham, G. Verma, P. C. Lan, C. Shan, H. Xing, K. A. Forrest, S. Suepaul, B. Space, A. Nafady, A. M. Al-Enizi and S. Ma, *Angew. Chem. Int. Ed.*, 2021, **60**, 5283—5288; (b) Z. Di, C. Liu, J. Pang, C. Chen, F. Hu, D. Yuan, M. Wu and M. Hong, *Angew. Chem. Int. Ed.*, 2021, **60**, 10828—10832; (c) M. L. Foo, R. Matsuda, Y. Hijikata, R. Krishna, H. Sato, S. Horike, A. Hori, J. Duan, Y. Sato, Y. Kubota, M. Takata and S. Kitagawa, *J. Am. Chem. Soc.*, 2016, **138**, 3022—3030;(d) P. Li, Y. He, Y. Zhao, L. Weng, H. Wang, R. Krishna, H. Wu, W. Zhou, M. O'Keeffe, Y. Han and B. Chen, *Angew. Chem. Int. Ed.*, 2015, **54**, 574—577.